





Cite this: *Digital Discovery*, 2025, 4, 1239

Machine learning-driven antiviral libraries targeting respiratory viruses†

Gabriela Valle-Núñez,  Raziel Cedillo-González, Juan F. Avellaneda-Tamayo, 
Fernanda I. Saldívar-González, Diana L. Prado-Romero  and José L. Medina-Franco *

Viral infections represent a significant global health concern. Viral diseases can range from mild symptoms to life-threatening conditions, and the impact of these infections has grown due to increased contagious rates driven by globalization. A prime example is the SARS-CoV-2 pandemic, which emphasized the urgent need to design and develop new antiviral drugs. This study aimed to generate a curated data set of compounds relevant to respiratory infections, focusing on predicting their antiviral activity. Specifically, the study leverages ML classification models to evaluate focused and on-demand compound libraries targeting pathways associated with viral respiratory infections. ML models were trained based on the antiviral biological activity related to respiratory diseases deposited on a major public compound database annotated with biological activity. The models were validated and retrained to classify and design antiviral-focused libraries on seven respiratory targets.

Received 24th January 2025

Accepted 2nd April 2025

DOI: 10.1039/d5dd00037h

rsc.li/digitaldiscovery

1 Introduction

Viral infections can range from mild, self-limited illnesses to severe, human life-threatening diseases.¹ In an era of increased global interdependence, climate change, forced migration and intensified globalization, the rapid replication and high contagion rates of viruses have become a critical concern. The resurgence of infections once believed to be under control, driven by viral genetic mutations and anti-vaccine movements, has further heightened the threat of deadly pandemics.² To combat this global health crisis, there has been a renewed focus on drug development strategies. The World Health Organization (WHO) has emphasized the challenge posed by limited resources for disease research and development, particularly given the vast array of potential pathogens. WHO has established a prioritized list of diseases with the greatest public health impact, based on their epidemic potential and the lack of effective countermeasures.³ This list is further detailed by the WHO's document "Pathogens Prioritization" which outlines the viral families and their respective members considering the risk of causing Public Health Emergencies of International Concern (PHEICs) or a pandemic (Table S1†).⁴⁻⁶

Despite ongoing efforts, developing effective antivirals for most viruses remains a significant challenge due to several key obstacles in antiviral discovery. These include the identification

of specific targets, narrow treatment windows, vector spread and control, and the emergence of mutations that contribute to antiviral resistance.⁷ In response, there has been a growing focus on developing structurally diverse antivirals with enhanced safety profiles, as well as those that retain efficacy against drug-resistant strains. This shift in focus has led to renewed interest in compounds with novel mechanisms of action.⁸

Acute respiratory disease (ARD) represents a significant portion of acute illnesses and fatalities worldwide. Acute viral respiratory tract infections alone are responsible for approximately 80% of ARD cases.⁹ Key viral pathogens in this category include influenza, respiratory syncytial virus (RSV), coronaviruses, adenovirus, and rhinovirus, all of which are related to some of the most highlighted diseases on the WHO's prioritized list (Table S1†). While viruses like adenovirus and rhinovirus typically result in lower mortality rates, they contribute substantially to morbidity and place a significant economic burden on healthcare systems.¹⁰

The emergence of highly pathogenic coronaviruses, such as the SARS-CoV-2 virus, responsible for the COVID-19 pandemic, has highlighted the severe threat posed by these pathogens. Other coronavirus strains, including those that caused the Severe Acute Respiratory Syndrome (SARS) and Middle East Respiratory Syndrome (MERS) outbreaks, persist as significant public health risks, and place substantial pressure on healthcare systems, especially in regions with high comorbidity rates and limited financial resources.^{11,12}

The COVID-19 pandemic represented one of the most significant threats to global health and stability in recent

DIFACQUIM Research Group, Department of Pharmacy, School of Chemistry, Universidad Nacional Autónoma de México, Avenida Universidad 3000, Mexico City 04510, Mexico. E-mail: medinajl@unam.mx; Tel: +52-55-5622-3899

† Electronic supplementary information (ESI) available. See DOI: <https://doi.org/10.1039/d5dd00037h>



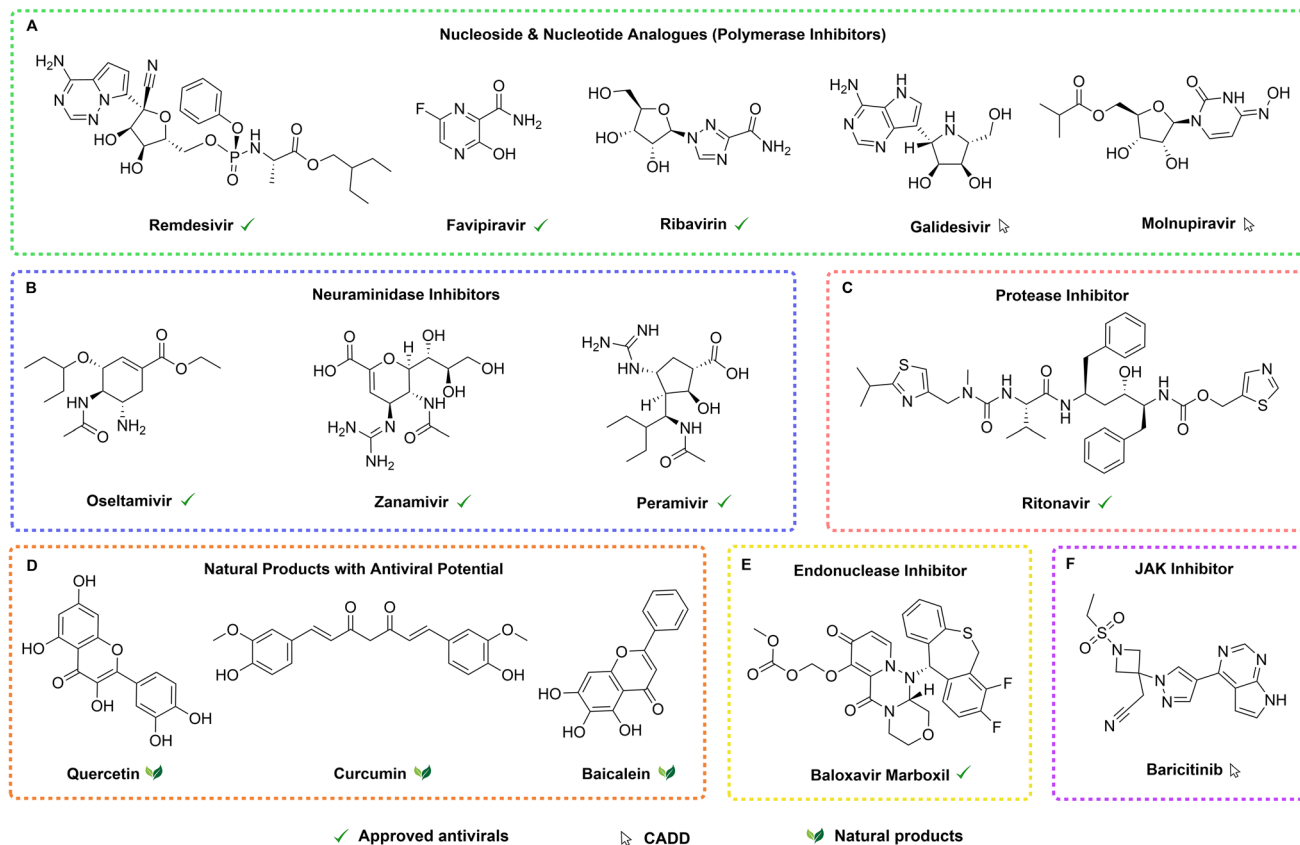


Fig. 1 Compounds with antiviral activity against targets associated with respiratory infections, identified or developed from different sources. (A) Inhibit viral RNA-dependent RNA polymerase (RdRp), preventing viral replication. (B) Block the viral neuraminidase enzyme, preventing viral release from infected cells. (C) Inhibit viral proteases required for processing viral polyproteins. (D) Plant-derived compounds with antiviral activity through various mechanisms. (E) Inhibits viral cap-dependent endonuclease, blocking viral mRNA synthesis. (F) Blocks the JAK-STAT signaling pathway, reducing excessive immune responses.

history, triggering an unprecedented surge in antiviral drug and vaccine research, alongside broader innovations in healthcare and daily life. Antiviral development integrates a diverse array of strategies, spanning well-established therapeutic approaches and emerging targeted interventions.¹³ This field draws upon both synthetic and natural sources, yielding compounds that exhibit a wide range of chemical structures and mechanisms of action, including direct inhibition of viral replication, immune system modulation, and disruption of host-virus interactions.^{14–16}

Guo *et al.* reviewed recent advances in natural products (NPs) for antiviral research, with a particular focus on addressing drug resistance.¹⁶ Various NPs target essential viral enzymes such as integrase, reverse transcriptase, and protease.¹⁷ Flavonoids and polyphenols constitute the largest group of antiviral NPs, followed by diterpenes and triterpenes, with fewer examples found among alkaloids.¹⁸ Examples of plant-derived compounds with demonstrated antiviral properties are quercetin, curcumin, and baicalein. Quercetin has shown effectiveness against RSV, MERS-CoV, influenza, and rhinoviruses through inhibition of viral entry and replication.¹⁹ Curcumin has been proven to inhibit the SARS-CoV-2 spike glycoprotein, ACE2 receptor, and proteases.²⁰ *Scutellaria baicalensis* root

extract is traditionally used in Asia, as an antiviral, antioxidant, and anti-inflammatory. This extract contains baicalein, which has demonstrated inhibition of SARS-CoV-2 main protease (Mpro) activity and viral replication *in vitro* (Fig. 1).^{21,22}

Drug repositioning of approved drugs and advanced stages developing molecules has also played a key role in the development of novel antivirals with known molecules, as is the case of SARS-CoV-2.^{23,24}

Computer-aided drug design (CADD) has significantly advanced antiviral discovery. Liao *et al.* identified five natural compounds – narcissoside, kaempferol-3-*O*-gentiobioside, rutin, vicin-2, and isoschaftoside – as potential SARS-CoV-2 Mpro inhibitors.²⁵ Generative topographic mapping (GTM) has aided in identifying antiviral motifs and screening virtual chemical libraries, as demonstrated in the design of anti-herpes compounds (herpes simplex virus type 1).^{26,27} CADD methods have also identified several promising antiviral compounds. These include baricitinib, galidesivir, and molnupiravir. Baricitinib was predicted by artificial intelligence (AI)-driven analysis to inhibit viral entry and inflammation in SARS-CoV-2.²⁸ Galidesivir, an antiviral for Ebola and Zika, was evaluated through structural modeling as a potential inhibitor of SARS-CoV-2 RdRp.²⁹ Molnupiravir (EIDD-2801), a prodrug of β -D-*N*₄-



hydroxycytidine, was optimized through docking and molecular dynamics to interfere with SARS-CoV-2 replication (Fig. 1).³⁰ Approved antivirals such as remdesivir, favipiravir, and ritonavir have been repurposed for respiratory viruses through virtual screening (VS), further confirming their potential to inhibit RNA polymerases (Fig. 1).³¹

Focused virtual libraries of compounds are valuable resources for bioactive compound discovery. These libraries compile data on molecules with potential biological activity, identified through ligand-based and structure-based drug discovery approaches. They play a crucial role in prioritizing candidates for synthesis, biological evaluation, and efficient allocation of resources. Notable recent examples of disease-specific focused virtual libraries include those targeting neglected infectious diseases,³² SARS-CoV-2,^{33,34} Sirtuin-1 dysregulation,³⁵ and type 2 diabetes mellitus.³⁶

Given the ongoing demand for respiratory-focused antivirals, extensive research has generated a wealth of structure-activity data available in public repositories such as ChEMBL.^{37,38} This data serves as a crucial input for machine learning (ML) models to design focused libraries for further experimental screening.

The main goal of this study was to design antiviral libraries focused on molecular targets related to respiratory diseases. To achieve this, we trained, retrained and validated ML classification models using bioactivity data from ChEMBL 33.^{37,38} The predictive models were used to filter compound libraries from diverse sources. As part of the data preparation to train the ML models, the chemical data sets were analyzed and characterized in terms of chemical diversity and coverage in chemical space using cheminformatics methods. The resulting antiviral-focused chemical libraries, which are freely available in the public domain, offer valuable starting points for further computational and/or experimental screening, which is the next logical step of this study.

2 Methods

The methodology followed in this study is outlined schematically in Fig. 2 and is detailed in the subsequent sections.

2.1 Data acquisition and preparation

Using the ChEMBL Application Programming Interface (API),³⁸ we retrieved all compounds from ChEMBL 33 (updated June 2023) associated with 13 viral targets linked to respiratory diseases. Molecular structures of these compounds were encoded in Simplified Molecular Input Line Entry System (SMILES) format.³⁹ A specific acronym was assigned to each virus with a target of interest, based on its strain, ensuring consistent and accurate identification throughout the analysis. Table 1 lists the names and target IDs for each of the 13 targets.

For compounds with multiple recorded biological activity values (“standard value”) against a target, we ranked these values from smallest to largest to ensure consistency in the data. The pIC_{50} was calculated for each compound, and compounds were classified according to the following criteria:

- (a) $IC_{50} \leq 10 \mu\text{M}$: were labeled as “Inhibitor”.
- (b) $10 \mu\text{M} < IC_{50} < 20 \mu\text{M}$: were labeled as “Unknown”.
- (c) $IC_{50} \geq 20 \mu\text{M}$: were labeled as “No_Activity”.

If a single category represented at least 80% of the recorded data for a compound, that category was used; otherwise, the label “Mixed” was assigned. Compounds with fewer than five data points retained their original classification, with “Mixed” assigned if they were labeled across multiple categories.

Additionally, one supplementary compound database was assembled, containing approved antivirals from DrugBank 5.1.12.⁴⁰ Compounds from ChEMBL associated with each viral target, along with those from DrugBank, were compiled into two collections.

A comprehensive data curation process was applied to data sets to ensure data integrity. Compounds with null values, empty entries, or duplicates were removed, resulting in a final count of 4521 compounds from ChEMBL 33, and 92 approved antivirals from DrugBank. Molecular structures were standardized using RDKit version 2024.03.5,⁴¹ and MolVS,⁴² following a well-established and used standardization protocol.⁴³ Data sets and code notebooks are publicly accessible through DIFACQUIM’s GitHub repository at https://github.com/DIFACQUIM/antiviral_ML.

2.2 Data modelability and target selection

To assess the feasibility of developing binary classification models, we calculated the modelability index (MODI), proposed by Golbraikh *et al.*⁴⁴ MODI measures the proportion of compounds in a data set whose nearest neighbor belongs to the same class within a defined feature space. We calculated the MODI values for the ChEMBL data sets using Molecular ACCESS System (MACCS) keys (166 bits)⁴⁵ and Morgan Chiral of radius 2 (2048 bits) fingerprints,⁴⁶ using the RDKit, NumPy, pandas, and SciPy libraries for Python 3. For each target in the ChEMBL data sets, MODI was calculated using two approaches: (1) including compounds classified as “Mixed” in the overall classification, and (2) excluding them (Table S2†).

Target selection for predictive model development was guided by the criteria established by Sánchez-Cruz and Medina-Franco.⁴⁷ According to these guidelines, a target was deemed suitable for predictive modeling if it included at least 30 active and 30 inactive compounds, and if it had a MODI score of 0.7 or higher for at least one molecular representation. Based on these criteria, we selected the seven targets listed in Table S2† for the construction of predictive models.

2.3 Chemoinformatic characterization of training data sets of selected targets

For each training data set of selected targets, active compounds were collected to perform a chemoinformatic characterization, detailed hereunder.

2.3.1 Data visualization of physicochemical and constitutional properties. For each active molecule in each data set of selected targets, physicochemical properties of pharmaceutical interest and constitutional descriptors were computed with Python language using RDKit toolkit version 2024.03.06 and



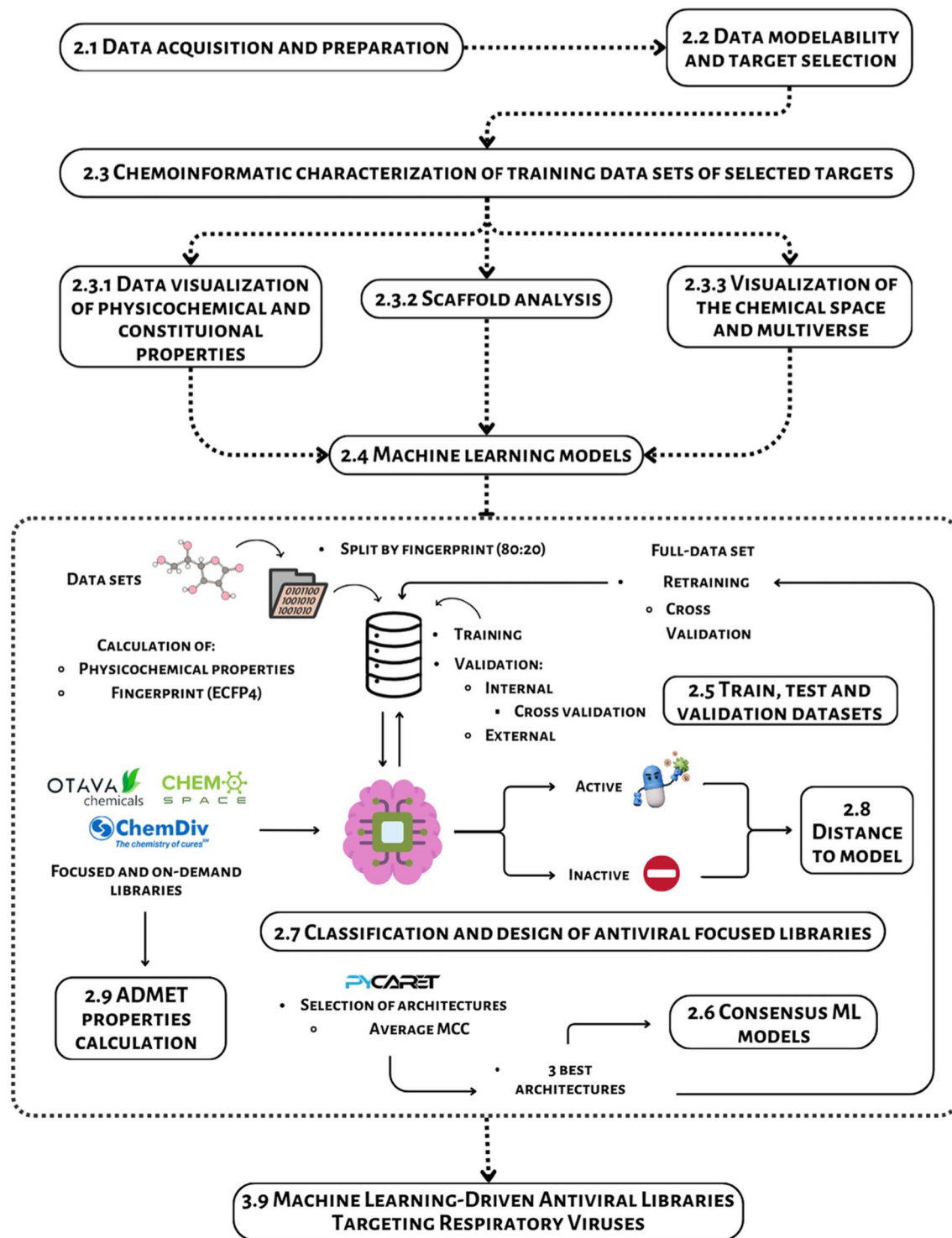


Fig. 2 Workflow followed in this study to design antiviral focused libraries.

Molecular Operating Environment (MOE), version 2022.02,⁴⁸ to analyze their distribution so as to compare it with approved antivirals from DrugBank. Utilizing RDKit's "Descriptors" module, 15 physicochemical and constitutional properties were computed: number of H-bond acceptors (HBA), number of H-bond donors (HBD), partition coefficient octanol/water ($\log P$), topological polar surface area (TPSA), molecular weight (MW),

number of saturated rings, fraction of sp^3 carbon atoms (CSP3), number of heavy atoms, number of rings systems, number of alicyclic rings formed by carbon atoms, number of alicyclic rings that include heteroatoms, number of heteroatoms, rotatable bond fraction, number of aromatic rings formed by carbon atoms, number of aromatic rings that include heteroatoms. Additionally, 11 descriptors were calculated using MOE: the



Table 1 Viral targets associated with respiratory diseases considered in this work

Family	Virus	Acronym	ChEMBL target ID
Coronaviridae	Feline coronavirus	FCoV	CHEMBL612744, CHEMBL4295624
	Human coronavirus 229E	HCoV-229E	CHEMBL613837, CHEMBL4888440
	Human coronavirus NL63	HCoV-NL63	CHEMBL3232683
	Middle East respiratory syndrome-related coronavirus	MERS-CoV	CHEMBL4296578, CHEMBL4295557
	Severe acute respiratory syndrome coronavirus	SARS-CoV	CHEMBL4802007
Coronaviridae	Severe acute respiratory syndrome coronavirus 2	SARS-CoV-2	CHEMBL4888460, CHEMBL5169223, CHEMBL4303835
	Enterovirus A71	HEV-71	CHEMBL612436, CHEMBL4295606, CHEMBL4295525
Picornaviridae	Human rhinovirus	HRV	CHEMBL613760, CHEMBL2857, CHEMBL612470
	Human parainfluenza virus 1	HPIV-1	CHEMBL1764934
Paramyxoviridae	Human respiratory syncytial virus	HRSV	CHEMBL4635143, CHEMBL2364165, CHEMBL4630897
Orthomyxoviridae	<i>Influenza A virus</i>	IAV	CHEMBL613740, CHEMBL612610, CHEMBL2367089
	<i>Influenza B virus</i>	IBV	CHEMBL613129, CHEMBL4295840, CHEMBL2028641
Paramyxoviridae	<i>Henipavirus nipahense</i>	NiV	CHEMBL6047, CHEMBL615055

number of acid atoms, aromatic atoms, basic atoms, nitrogen, oxygen, bromine, chlorine, fluorine, iodine, the fraction of rotatable bonds, and the number of chiral centers.

2.3.2 Scaffold analysis. Scaffolds were generated using the Bemis–Murcko definition using RDKit's "MurckoScaffold" module, which consists of removing all side chains in molecules and preserving the ring systems and their linkers.⁴⁹ To remark on the most frequent scaffolds, including acyclic molecules, we counted and ordered them from highest to lowest, then calculated their proportion on the data set.

2.3.3 Visualization of the chemical space and multiverse. Visualization of the chemical space and chemical multiverse (e.g., chemical space based on different molecular representations) was conducted for each data set of selected targets using *t*-distributed stochastic neighbor embedding (*t*-SNE) based on MACCS keys (166 bits) and Morgan Chiral of radius 2 (2048 bits) fingerprints. The chemical multiverse of compounds with antiviral activity by each pre-selected target was compared with approved antivirals from the DrugBank data set. *t*-SNE analysis was implemented utilizing the Python library Scikit-Learn version 1.5.211 (ref. 50) and the code is freely available from DIFACQUIM's GitHub repository at https://github.com/DIFACQUIM/antiviral_ML.

2.4 Machine learning models

To transform the activity data into a binary format, compounds labeled as "Mixed" and "Unknown" in the ChEMBL data set were discarded, yielding two classes: "Inhibitor" = 1 and "No_Activity" = 0. Then, we computed Morgan Chiral of radius 2 (2048 bits) fingerprint with RDKit,⁴⁶ and 19 drug-likeness descriptors from the Datamol library.⁵¹ These descriptors included Lipinski-related parameters⁵² and other descriptors of pharmaceutical relevance: MW, CSP3, HBA, HBD, number of rings, number of heteroatoms, number of heavy atoms, number of rotatable bonds, TPSA, log *P*, number of aliphatic carbocycles, number of aliphatic heterocycles, number of aliphatic

rings, number of aromatic carbocycles, number of aromatic heterocycles, number of aromatic rings, number of saturated carbocycles, number of saturated heterocycles, and number of saturated rings.

Only data corresponding to the seven selected targets (Table S2†) was filtered for model building. To evaluate and reduce multicollinearity, the Pearson correlation between descriptors was computed. The second descriptor was discarded if any pair showed a correlation above 0.8, prioritizing drug-likeness relevance.

For supervised binary classification modeling, we employed PyCaret version 3.3.2 for Python to develop models using 15 different ML algorithms (Table S3 in the ESI†).⁵³ Each model was trained on ChEMBL data for the selected targets, associated with a binary activity label (active/inactive). Morgan Chiral of radius 2 (2048 bits) fingerprint and physicochemical descriptors were used as molecular representation, with PyCaret's default hyperparameter settings.

Normalization, fold generation, and imbalance correction were achieved using *z*-score normalization, stratified *k*-fold cross-validation, and the Adaptive Synthetic Sampling (ADASYN) algorithm, respectively.⁵⁴ Additionally, we mitigated the risk of overfitting by enabling an early stopping mechanism to ensure that the models remain capable of generalizing well to new data points.

2.5 Training, test, and validation data sets

The predictive models generated for each target were evaluated by internal and external validations. Data sets were divided into training (80%) and test (20%) sets, using DeepChem library for Python,^{55,56} selecting Morgan Chiral of radius 2 (1024 bits) fingerprint. The internal validation of all the models was conducted by cross-validation, in which a new training/testing split multiple times from the available data is chosen. The external validation of all the models was conducted with the 20 percent of unseen testing properties. For both validations, the following



Table 2 Chemical libraries for VS in antiviral activity identification

Database	Acronym	Description	Compounds after curation
ChemDiv coronavirus library ⁵⁸	ChD_covL	Collection of small molecules with potential antiviral activity against coronavirus	20 750
ChemDiv antiviral library ⁵⁹	ChD_AvL	Collection of small molecules with potential antiviral activity, targeting over 50 key proteins in viruses	64 958
OTAVA drug-like green collection ⁶⁰	OT_DLGC	Drug-like green collection compound library, curated based on screening compounds for prompt delivery and pre-formatted according to Lipinski's rule of five	169 356
Enamine antiviral library ⁶¹	Ena_AvL	Collection of molecules designed for discovery of new nucleoside-like antivirals	3200
ChemSpace discovery diversity set ⁶²	ChE_DDS	Collection of small molecules that are synthesized from in-house building blocks using carefully developed and optimized reactions	10 000
LifeChemicals helicase targeted library ⁶³	LC_HTL	Collection of structurally diverse molecules with potential activity against key helicase-related drug targets, selected by a cheminformatics team through <i>in silico</i> molecular docking	3291
LifeChemicals helicase focused library ⁶³	LC_HFL	A curated collection of compounds targeting helicases, including viral and genetic disorder-related enzymes like hepatitis C NS3 and Werner syndrome helicases. Compounds were selected based on structural similarity (84% Tanimoto threshold)	3665
LifeChemicals 2019-nCoV papain-like protease (PLP) targeted library ⁶⁴	LC_plpL	A curated collection of drug-like compounds designed to target the PLP of SARS-CoV-2, using docking-based screening without constraints. Compounds were filtered for binding accuracy and removed if they were PAINS, toxic, or reactive	1736
LifeChemicals DNA polymerase targeted library ⁶⁵	LC_dptL	Library of structurally diverse compounds targeting DNA polymerase-related drug targets, developed using pharmacophore-driven screening	628
LifeChemicals polymerase focused library 15 polymerase assays ⁶⁵	LC_polL	A library of molecules identified for potential polymerase inhibition, created by screening 4567 active compounds from 15 polymerase assays targeting RNA and DNA polymerases. Compounds were selected using Tanimoto similarity from the life chemicals HTS compound collection and ranked by predicted activity	15 676
LifeChemicals polymerase focused library similarity to ChEMBL database ⁶⁵	LC_polSL	A library of drug-like screening compounds selected through a 2D fingerprint similarity search (Tanimoto index > 85%) against a reference set of 20 000 compounds from the ChEMBL database, all with reported activity against DNA and RNA polymerase targets	13 608
LifeChemicals SARS coronavirus focused library ⁶⁶	LC_covL	A curated collection of small-molecule compounds selected through a 2D fingerprint similarity search, targeting key SARS-CoV proteins. The compounds were chosen based on activity criteria from a reference set of 300 known SARS inhibitors	436
LifeChemicals 2019-nCoV main protease targeted library ⁶⁷	LC_mproL	A curated collection of drug-like compounds designed to target the main protease of SARS-CoV-2, using docking-based screening without constraints. Toxicophore filters were applied, while peptide-like structures were retained to enhance binding potential	2338
LifeChemicals antiviral targeted library ⁶⁸	LC_AVL	A curated library of diverse compounds identified through structure-based screening, targeting antiviral proteins like hepatitis B core protein and influenza A PA endonuclease. Developed using phase modeling and life chemicals' HTS collection, with customization options available	1350
LifeChemicals merged antiviral screening superset ⁶⁹	LC_MASS	Data set of small-molecule compounds consolidated into individual screening subsets for various viral diseases, providing a comprehensive resource in one collection	45 546
LifeChemicals antiviral library combined ligand-based and structure-based approaches ⁷⁰	LC_ALCLBSBA	A curated library of potential antiviral agents, designed using protein crystal structures of key viral targets. Selected through glide docking and UNITY pharmacophore searches, with PAINS and reactive compounds excluded	3514
LifeChemicals antiviral screening compound library 2D similarity ⁷⁰	LC_ASCL2DS	The antiviral screening compound library was designed using a 2D fingerprint similarity search against a reference set of 46 518 biologically active compounds from therapeutically relevant viral assays, covering various virus species and their target proteins	15 455
LifeChemicals bioactive compound library ⁷¹	LC_BCL	A collection of structurally diverse screening compounds, each with confirmed biological activity against approximately 600 pharmaceutical targets	9897



Table 2 (Contd.)

Database	Acronym	Description	Compounds after curation
LifeChemicals EF1A targeted library GDP site ⁷²	LC_gdp	Library that includes compounds selected through docking-based VS of GDP site on the eEF1A protein. The compounds have high predicted affinity, are Ro5-compliant, and exclude PAINS, toxic, or reactive groups. Subsets for each binding site are provided with docking scores	1267
LifeChemicals EF1A targeted library EF1B site ⁷³	LC_ef1b	Library that includes compounds selected through docking-based VS of EF1B site on the eEF1A protein. The compounds have high predicted affinity, are Ro5-compliant, and exclude PAINS, toxic, or reactive groups. Subsets for each binding site are provided with docking scores	1544
LifeChemicals pre-plated coronavirus COVID-19 screening set-384 well ⁷³	LC_cov19	Screening set consists of drug-like compounds from the 2019-nCoV Mpro targeted library, designed to support anti-coronavirus drug discovery efforts	2300
LifeChemicals preplated helicase screening set 6080 cmpds 384 well ⁷³	LC_PHSS384	Screening sets that include drug-like small-molecule compounds with potential helicase-related activity for drug discovery targeting infectious diseases and cancer. Alternatively, two smaller, non-overlapping subsets of 3520 and 2560 helicase-focused molecules are also available for separate purchase	6080
General screening antiviral data set ^a	VS data set	Data set containing only unique structures from all chemical libraries	339 040

^a Number of compounds before curation: 396 595.

metrics were calculated with PyCaret: accuracy, Area Under the Curve (AUC), recall, precision, F_1 score, kappa, Matthew's Correlation Coefficient (MCC) and Balanced Accuracy (BA). All seven metrics are statistical indicators of quality, used for model evaluation, offering insight into prediction accuracy with a focus on the active class.⁵⁷

For both validations, we obtained the MCC and calculated its average for all models, so as to select the three best architectures for the data sets studied in this analysis (Table S4†). MCC is a robust metric for assessing the quality of binary classification models, ranging from -1 to 1 . A value of 1 indicates perfect classification, 0 corresponds to random predictions, and -1 represents completely inverse predictions. The architectures selected for modeling were retrained on the complete data set corresponding to each target, aiming to significantly enhance the MCC and improve model generalization by optimizing performance. This retraining process utilized the same hyperparameters as those in the initial model construction and was applied to predict the final antiviral activity class of the data set assembled for VS, as described in Section 2.7. Cross validation was performed to assess the effectiveness of this retraining by obtaining the MCC retraining value.

2.6 Consensus ML models

For each target, the three top-performing ML models selected and retrained as outlined in Section 2.5, were combined to generate a consensus model. These consensus models underwent internal validation through cross-validation to calculate the MCC value using Scikit-Learn⁵⁰ functions, enabling performance comparison with each individual model.

2.7 Classification and design of antiviral focused libraries

In order to classify and design antiviral-focused libraries, first a total of 22 diverse focused and commercial chemical libraries from various online sources (Table 2) were compiled. The assembled database contained 339 040 compounds after curation (Table 2), that were classified and filtered using the predictive models developed for each target to assign a final antiviral activity class (see Section 2.5).

2.8 Distance to model

To establish a quantitative measure that relates to the applicability domain of the classification models, the similarity or distance for each predicted molecule to the training set was computed. Since the models were constructed using Morgan fingerprints and physicochemical properties, two types of similarity metrics were calculated. Jaccard distance was calculated using Morgan Chiral of radius 2 (2048 bits) fingerprint. While physicochemical properties' distance to the model was calculated with Euclidean distance, based on the preserved drug-like descriptors for each model architecture during the construction process, as outlined in Section 2.4. All predictions were categorized into four quartiles based on their mean Jaccard or Euclidean distance, as appropriate, from the compounds in the retraining set.⁷⁴ To assess this quartile, the mean distance between the predicted molecule and all compounds in the retraining set was compared with the resulting quartiles from the intraset distances of the corresponding retraining set. If the resulting distance fell into the distances from the training set, the same quartile was assigned; otherwise, the predicted compound was labeled as "Out."



2.9 ADMET properties calculation

Absorption, distribution, metabolism, excretion, and toxicity (ADMET) properties were calculated for the VS data set, generated by the assembly of focused and commercial libraries (see Section 2.7). This was accomplished using ADMET-AI,^{75,76} utilizing the Python library for local predictions. ADMET-AI computes eight physicochemical properties with RDKit and predicts forty-one ADMET properties through its Chemprop-RDKit graph neural networks.

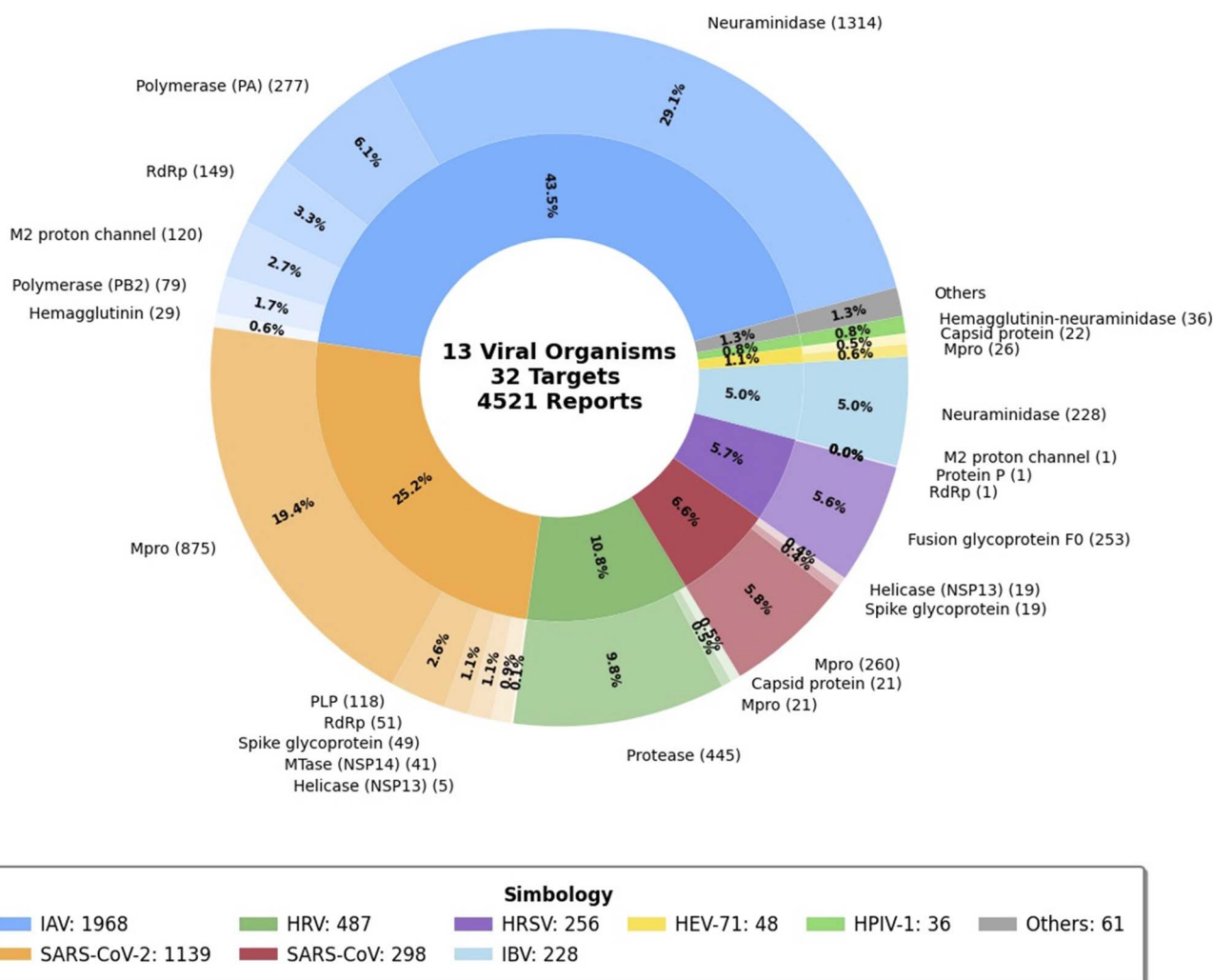
3 Results and discussion

3.1 Data acquisition and preparation

Fig. 3 presents an overview of the initial data set, which includes 4521 compounds retrieved from ChEMBL 33. These compounds are associated with 32 distinct viral targets across 13 viruses

implicated in respiratory infections. Among these, IAV is the most represented, with 1968 compounds, followed by SARS-CoV-2, with 1139 compounds. This distribution underscores a predominant research focus on these viruses, likely driven by their significant global impact, recurrent outbreaks, and the prioritization of pandemic-related research efforts. Indeed, the data set highlights a strong emphasis on highly studied targets such as proteases and polymerases, which play critical roles in viral replication and are central to current antiviral strategies. Conversely, targets with minimal representation, such as helicases and spike glycoproteins, represent potential gaps in current research and may offer promising avenues for future drug discovery. Interestingly, the inclusion of compounds targeting less-studied (or reported in ChEMBL) viruses, such as HRV (487 compounds) and IBV (228 compounds), indicates a growing interest in broad-spectrum antiviral strategies. This trend suggests a shift towards addressing a wider range of

Distribution of Viral Target Organisms



respiratory viruses, which could enhance preparedness for emerging infections.

3.2 Data modelability and target selection

As summarized in Table 3, seven out of 32 targets related to respiratory diseases were selected according to the criteria detailed in Section 2.2. Although the IAV M2 proton channel target did not meet the criterion of having at least 30 inactive compounds, it was selected as a test case to explore the implications of this criterion. This decision was based on the observation that many targets in the data set faced similar limitations—failing to meet the required number of active or inactive compounds—yet still achieved a MODI score of 0.7 or higher. The premise was that models built for such targets might exhibit different performance characteristics. The details of this analysis and its implications are further discussed in Section 3.4.

Targets such as SARS-CoV-2 Mpro and IAV neuraminidase exhibited the highest MODI scores (0.88 for MACCS keys (166 bits) and 0.91 for Morgan Chiral of radius 2 (2048 bits)), indicating strong modelability. In contrast, targets like SARS-CoV Mpro, which was selected for its relatively higher MODI score with Morgan Chiral of radius 2 compared to MACCS keys, or IBV neuraminidase, which had lower MODI scores (0.72 for MACCS keys and 0.71 for Morgan Chiral of radius 2), suggest potentially more challenging modelability. Notably, when comparing the performance of the two fingerprints, most targets showed slightly better modelability with Morgan Chiral of radius 2, suggesting that these fingerprints capture relevant chemical features more effectively for these targets.

The ratio of active to inactive compounds also appears to influence the MODI score. For instance, IAV neuraminidase, with a high number of both active (733) and inactive (390) compounds, had a correspondingly high MODI score. Additionally, the relationship between the median pIC_{50} values and the MODI scores is worth highlighting. For example, SARS-CoV-2 Mpro, with the highest median pIC_{50} value (6.35), aligned with its strong modelability, whereas targets with lower pIC_{50} values may exhibit more variable performance. Similarly, the total number of compounds may serve as another important indicator of modelability. For example, SARS-CoV-2 Mpro, with the second largest data set, likely benefits from a richer data set for model training. Conversely, smaller data sets, such as IAV M2 proton channel, may result in reduced predictive performance due to limited data diversity, as discussed further in the next

sections. It is also notable that targets, such as IBV neuraminidase, had lower MODI scores despite a reasonably balanced data set. This discrepancy could be attributed to factors such as structural complexity or compound heterogeneity, which may pose additional challenges for predictive modeling.

3.3 Chemoinformatic characterization of training data sets

For the seven selected data sets, we performed a characterization of the structural content, diversity and coverage in chemical space using different structural representations and descriptors (*e.g.*, chemical multiverse).

3.3.1 Analysis of physicochemical and constitutional properties. Fig. S1 in the ESI† shows boxplots of the distributions of ten physicochemical properties, including those related to drug-likeness as defined by Lipinski's "Rule of Five". Table S5† summarizes the calculated physicochemical properties and other constitutional descriptors along with their statistical metrics across the data sets. When comparing the distributions of the calculated properties against the reference set of approved antiviral drugs, it was observed that most of the analyzed compounds exhibit physicochemical properties compatible with Lipinski's Rule of Five. Exceptions were identified, most notably in compounds targeting IAV polymerase (PA), which deviated from the drug-likeness parameters and did not match with the approved antivirals data set. These deviations could be attributed to the unique structural or functional requirements of compounds targeting this specific viral protein.

It is important to emphasize that the ML models were constructed using different sets of physicochemical properties tailored to each target. This variation could significantly influence the data modelability, as certain properties might be more relevant for specific viral targets. For future research, exploring the impact of these individual properties on the performance of the models could provide deeper insights and help refine predictive frameworks.

3.3.2 Scaffold analysis. An analysis of the most frequent structural scaffolds present in the data sets with known biological activity (training data sets), shown in Fig. 4, revealed notable trends among the targets. For instance, the HRV protease and the IAV M2 proton channel share at least one scaffold with the set of approved antivirals. Additionally, the neuraminidases from influenza types A and B were found to share common scaffolds, despite the generally low percentage of sequence homology reported between them.⁷⁷ Interestingly,

Table 3 Targets selected based on the modelability index (MODI) criteria

Target	Organism	Count	pIC_{50} median	Active	Inactive	MODI MACCS keys (166 bits)	MODI Morgan Chiral of radius 2 (2048 bits)
M2 proton channel	IAV	92	5.45	68	24	0.82	0.83
Mpro	SARS-CoV	197	4.52	77	120	0.66	0.77
	SARS-CoV-2	815	6.35	651	164	0.88	0.91
Neuraminidase	IAV	1123	5.72	733	390	0.88	0.91
	IBV	202	5.47	132	70	0.72	0.71
Polymerase (PA)	IAV	256	5.40	151	105	0.84	0.88
Protease	HRV	389	5.96	298	91	0.83	0.85



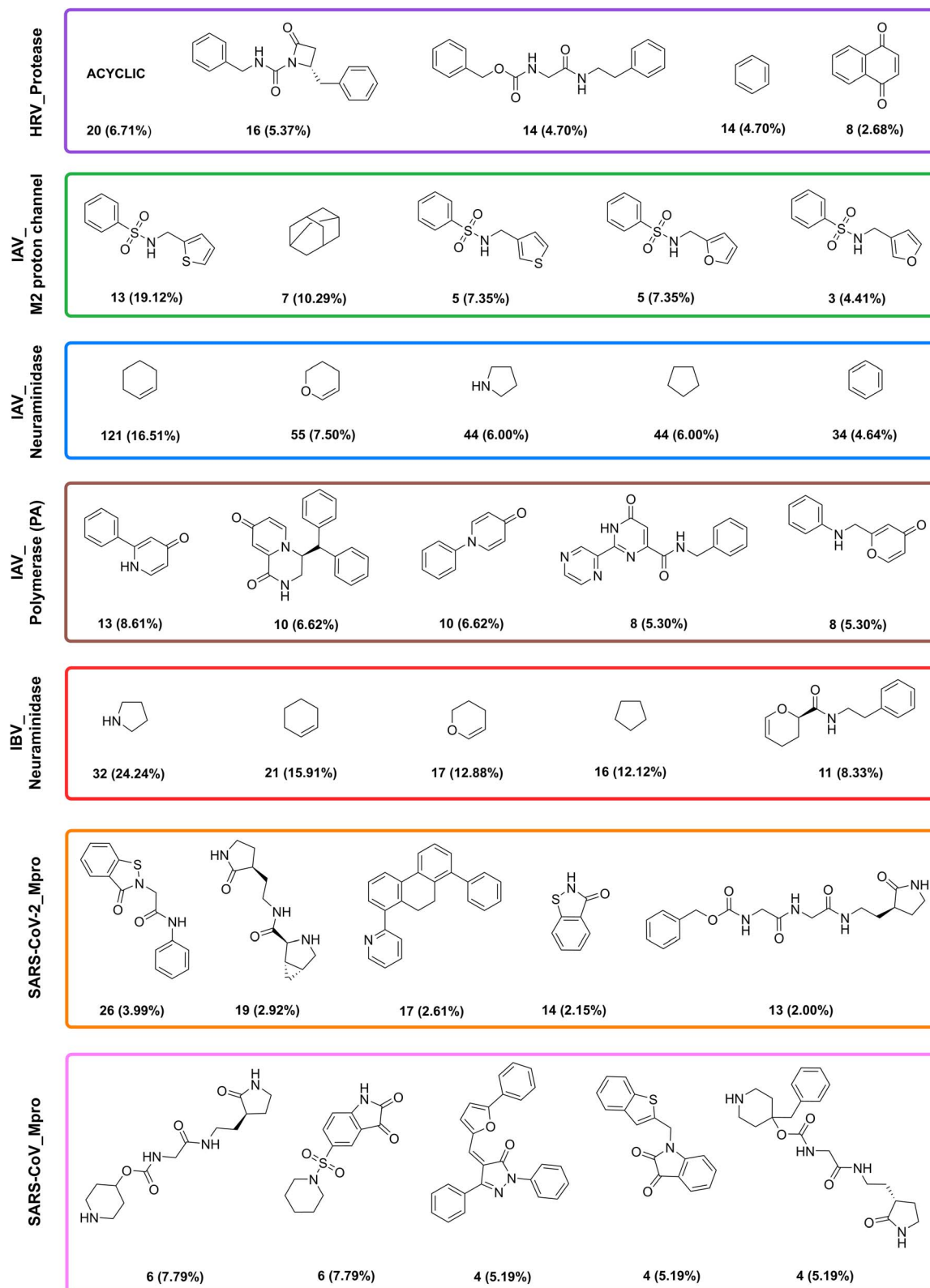


Fig. 4 Absolute and relative percentage frequencies of the most frequent scaffolds in compounds with known activity for seven selected antiviral targets. Prominent scaffolds are categorized by target, highlighting key structural features in the data set used for ML model development.



these shared scaffolds are predominantly single-ring structures, which may indicate a tendency toward compounds with lower MW within these data sets. This observation could have implications for the drug discovery process, particularly in terms of scaffold-based design and the potential for optimizing molecular properties.

More details about the most frequent scaffolds in the training data sets for each target are illustrated in Fig. S2† after following the curation and standardization processes.

Antiviral drugs commonly exhibit diverse structural scaffolds, including adenine derivatives and privileged frameworks that facilitate interactions with multiple viral mechanisms. These compounds frequently feature key atoms such as nitrogen, oxygen, and carbon, which play critical roles in their biological activity and contribute to their structural diversity.⁷⁸

As presented in the ESI, Fig. S3† shows the most frequent ring systems in the training data sets, while Fig. S4 and S5† depict the predominant scaffolds and ring systems in the VS data set, respectively. Not surprisingly, the benzene ring was the most frequent scaffold and ring system, reflecting its ubiquitous presence across the chemical data set. Notably, the top ring systems in the VS data set has a high prevalence of nitrogen-containing rings, a feature that holds significant promise for enhancing antiviral activity due to their well-established role in molecular recognition and binding to viral targets.^{79,80}

3.3.3 Visualization of the chemical multiverse. Fig. 5 and S6† show visual representations of the chemical multiverse (*e.g.*, multiple chemical spaces, each defined by different representations) of the active compounds of the seven antiviral data sets (Table 3) and 92 antivirals in DrugBank. The chemical

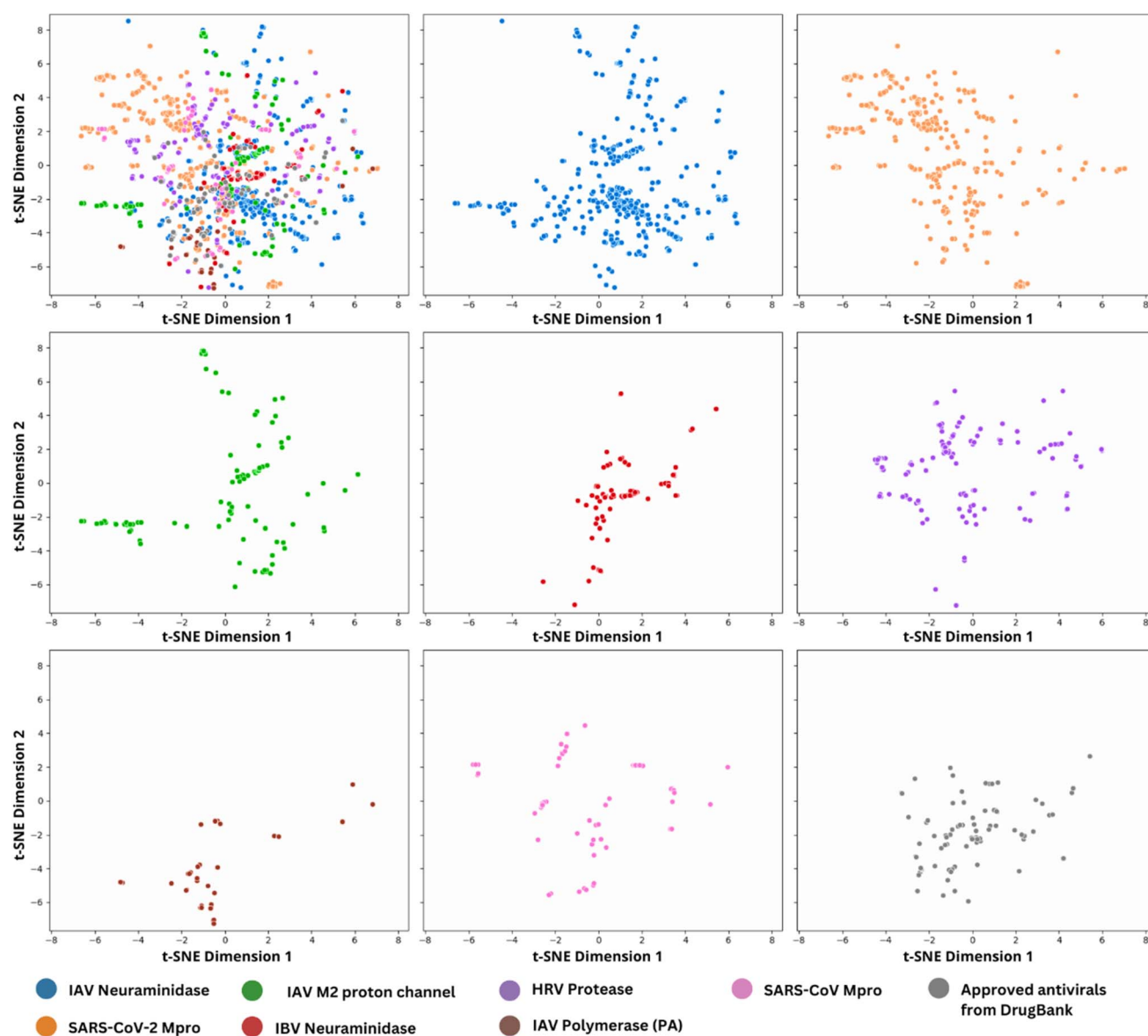


Fig. 5 Chemical multiverse visualization of seven antiviral data sets focused on different targets as compared with approved antivirals from DrugBank. The visualization is done with *t*-SNE using Morgan Chiral of radius 2 (2048 bits) fingerprint. On the upper left are illustrated super-imposed data sets, followed by individual data sets using the same coordinates for all of them.



multiverse is based on Morgan Chiral of radius 2 (2048 bits) (Fig. 5) and MACCS keys (166 bits) fingerprints (Fig. S6†). The visualization highlights distinct patterns in the chemical space. The distribution of active compounds in the chemical space emphasized the diversity of chemical scaffolds that may be associated with antiviral activity. This diversity was particularly evident in targets such as SARS-CoV-2 Mpro and IAV neuraminidase with large coverage of the chemical space. Furthermore, visualizations with both fingerprints suggest the presence of structurally similar compounds to approved antivirals within the active subset derived from the retraining phase. This overlap reinforces the predictive models' reliability in identifying bioactive compounds while also supporting the hypothesis that structurally similar compounds are likely to exhibit similar biological activity. A complementary visualization of the chemical multiverse is presented in Fig. S7,† featuring a general constellation plot⁸¹ centered on chemical scaffolds. This plot employs *t*-SNE for dimensionality reduction, with point sizes reflecting the number of compounds associated with each molecular scaffold and a color scale representing *p*IC₅₀ values reported in ChEMBL. This visualization offers valuable insights into the distribution and activity patterns of scaffolds within the chemical data set.

3.4 Machine learning models

Table S6 in the ESI† summarizes the MCC values from each validation phase for the top three best-performing architectures selected for each target. To determine the optimal model, we prioritized the MCC values obtained during the retraining phase (refer to Methods Section 2.4 for further details). As shown in Table S6,† MCC values improved in general after the retraining phase, with the AdaBoost model for IBV neuraminidase standing out as a particularly strong performer. These results showed the capability of the models to accurately

identify promising compounds, underscoring their potential utility in antiviral drug discovery.

According to the discussion of data modelability in Section 3.2, as expected, the IAV M2 proton channel target had the lowest MCC values for all three top models in each validation phase. This result emphasized the importance of the minimum amount of compounds and reinforced the relevance of implementing several criteria while selecting and analyzing molecular targets to develop reliable and useful ML models.

As illustrated in Fig. 6, some models were robust for a few targets at different validation phases but not in all of them. For instance, the AdaBoost classifier performed best for IBV neuraminidase during retraining while others like the Support Vector Machine (SVM – linear kernel) performed best for IAV polymerase (PA) during the internal validation of the training process. Moreover, this model showed consistent MCC values across training and retraining. This consistency suggests robust model performance and generalizability.

3.5 Consensus machine learning models

The three best-performing models discussed in Section 3.4 were combined to create a consensus model for each target. Table S6 in the ESI† summarizes the MCC values calculated for the consensus model in comparison with those obtained from each of the top three models individually. In general, the consensus models improved the MCC value or maintained it at a comparable level. This result underscored the robustness of combining predictions from diverse algorithms, which likely reduces individual model biases. Indeed, combining outcomes from complementary methodologies has shown advantages in several areas of cheminformatics.⁸² A notable improvement was obtained for SARS-CoV Mpro, where the consensus model surpassed the performance of any single model, further validating this approach as a reliable strategy for enhancing

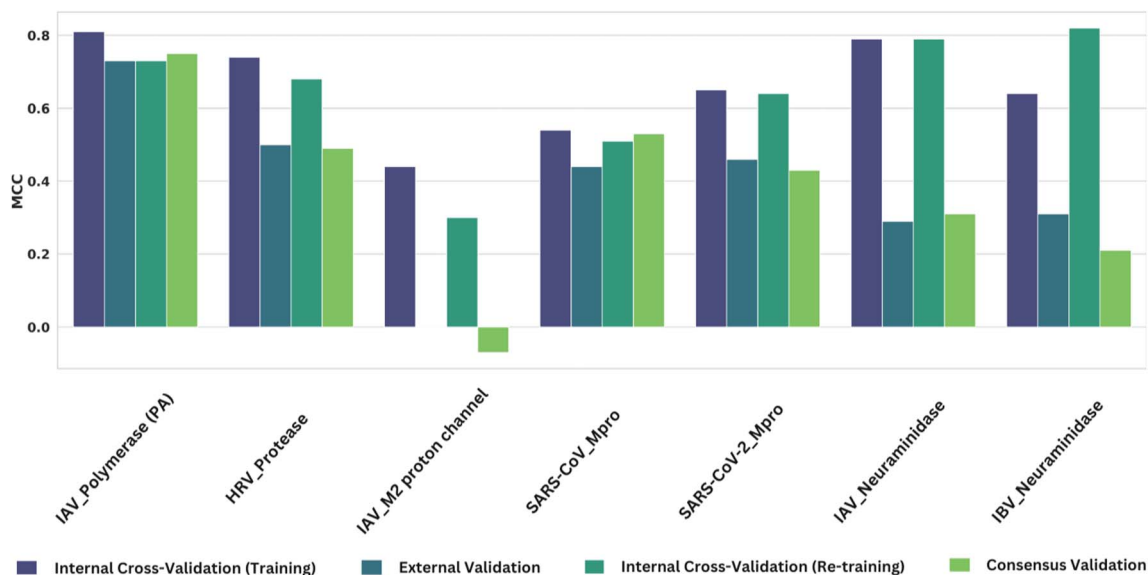


Fig. 6 Comparison of MCC per target, best-fit model (highlighted in yellow in Table S6†), and validation phase.



predictive accuracy. However, a few exceptions were noted. For example, the IAV M2 proton channel exhibited the lowest MCC value for the consensus model. This result aligns with previously discussed limitations for the IAV M2 proton channel, including the small and imbalanced data set (see Section 3.2 for further details). Such cases highlight that while consensus models generally provide stability and enhancement, their effectiveness depends on the quality and representativeness of the input data.

3.6 Classification of antiviral-focused libraries

The prediction of antiviral activity for the compounds from the assembled general screening data set (VS data set) (Table 2) led to the design of seven individual antiviral-focused libraries for each target. The design consisted in the calculation of two outputs using PyCaret's prediction function: binary values (0/1) for labeling, indicating whether a compound is predicted (classified) to be active (1) or inactive (0); and a prediction score, which represents the probability of the compound belonging to the active class (for further details, see Section 2.5). Table 4 summarizes the results of these predictions from the VS data set for the seven antiviral targets. The table includes the number of compounds predicted to be active by one, two, and three models and for the top, second, and third best models, as well as its relative frequency.

3.6.1 Distance to model. At the classification (prediction) step, the performance of the best individual model (highlighted in yellow in Table S6†) and the consensus model (highlighted in green in Table S6†) was assessed based on their distance-to-model, which serves as an estimation of the applicability domain of the models. Since all models were constructed using the Morgan Chiral of radius 2 (2048 bits) fingerprint and various physicochemical properties, the distance-to-model was evaluated separately for each representation. Descriptive statistics of both distances for each target are detailed in Table S7.† The compound's predictions were categorized into four quartiles based on their mean Jaccard or Euclidean distance from the compounds in the retraining set (see Methods Section 2.8 for further details). Table 5 summarizes the distribution of predicted compounds across these quartiles, as well as those falling out of the defined applicability domain, using the Morgan Chiral of radius 2 (2048 bits) fingerprint. Similarly, Table 6 presents the distribution of compounds using their corresponding preserved drug-like descriptors. The analyses in Tables 7 and S8† provide insight into how well the models generalize to novel compounds and highlight compounds lying beyond the applicability domain, which could serve as candidates for further experimental validation or re-evaluation of the models' chemical space coverage. Compounds on quartile 1 (Q1) should be prioritized for further analysis, including biological testing.

In general, fewer compounds are considered "Out" when the distance is calculated with physicochemical properties. This could be due to the preservation of drug-like properties for the commercial and focused libraries, and the ChEMBL compounds, as observed in Section 3.3.1. The results for IBV

Table 4 Number and proportion of compounds classified as active in the VS data set

Target	Number of predicted active compounds by ^a						Active	Third best model	Active	Third best model	Active
	3 models	2 models	1 model	Top best model	Second best model	Active					
IAV_polymerase (PA)	9234 (2.72)	11 272 (3.32)	26 409 (7.79)	SVM – linear kernel	22 295 (6.58)	26 444 (7.80)	27 916 (8.23)	Gradient boosting classifier	26 444 (7.80)	27 916 (8.23)	Gradient boosting classifier
HRV_protease	225 751 (66.59)	69 364 (20.46)	24 034 (7.09)	Gradient boosting classifier	302 149 (89.12)	284 152 (83.81)	253 714 (74.83)	AdaBoost classifier	284 152 (83.81)	253 714 (74.83)	AdaBoost classifier
IAV_M2 proton channel	13 296 (3.92)	174 286 (51.41)	146 457 (43.20)	Quadratic discriminant analysis	326 809 (96.39)	26 209 (7.73)	181 899 (53.65)	Dummy classifier	26 209 (7.73)	181 899 (53.65)	Dummy classifier
SARS-CoV_Mpro	16 660 (4.91)	46 894 (13.83)	103 702 (30.59)	Linear discriminant analysis	49 992 (14.75)	112 286 (33.12)	85 192 (25.13)	SVM – linear kernel	112 286 (33.12)	85 192 (25.13)	SVM – linear kernel
SARS-CoV-2_Mpro	169 434 (49.97)	79 272 (23.38)	52 692 (15.54)	Light gradient boosting machine	245 950 (72.54)	244 792 (72.20)	228 796 (67.48)	Decision tree classifier	244 792 (72.20)	228 796 (67.48)	Decision tree classifier
IAV_neuraminidase	8101 (2.39)	21 190 (6.25)	120 020 (35.40)	Logistic regression	133 100 (39.26)	33 079 (9.76)	20 524 (6.05)	Extra trees classifier	33 079 (9.76)	20 524 (6.05)	Extra trees classifier
IBV_neuraminidase	1054 (0.31)	32 091 (9.47)	137 600 (40.59)	AdaBoost classifier	162 085 (47.81)	3167 (0.93)	39 692 (11.71)	Extra trees classifier	3167 (0.93)	39 692 (11.71)	Extra trees classifier

^a Number in parenthesis is the relative percentage frequency.



Table 5 Distance to model performance of the retraining data set, the best classification model and consensus model for each selected target, attired by Morgan Chiral of radius 2 (2048 bits) fingerprint

Range	IAV_polymerase (PA)			SARS-CoV-2_Mpro		
	Total	Best model (actives)	Consensus (actives)	Total	Best model (actives)	Consensus (actives)
Out	4855	310	125	1162	881	593
Q1	11	—	—	3	2	2
Q2	660	44	16	3	2	1
Q3	14 083	926	410	19 210	13 975	9622
Q4	319 431	21 015	8683	318 662	231 090	159 216
Range	HRV_protease			IAV_neuraminidase		
	Total	Best model (actives)	Consensus (actives)	Total	Best model (actives)	Consensus (actives)
Out	2883	2569	1936	1162	476	35
Q1	404	371	268	3	1	—
Q2	3552	3224	2469	20	8	1
Q3	28 978	25 835	19 322	28 109	10 786	611
Q4	303 223	270 150	201 756	309 746	121 829	7454
Range	IAV_M2 proton channel			IBV_neuraminidase		
	Total	Best model (actives)	Consensus (actives)	Total	Best model (actives)	Consensus (actives)
Out	5277	5086	3537	320 156	152 989	997
Q1	2879	2776	1981	—	—	—
Q2	119 392	115 160	79 248	—	—	—
Q3	149 663	144 277	99 610	2	1	—
Q4	61 829	59 510	41 375	18 882	9095	57
Range	SARS-CoV_Mpro					
	Total	Best model (actives)	Consensus (actives)			
Out	1506	210	55			
Q1	83	12	2			
Q2	11 376	1676	597			
Q3	195 827	28 807	9526			
Q4	130 248	19 287	6480			

neuraminidase had the greatest number of compounds labeled as “Out” for both distances. This is aligned with the MODI results since IBV neuraminidase was the target with the lowest value for fingerprints.

3.7 ADMET properties profiling of antiviral-focused libraries

Among the main reasons for antiviral drug failure are issues related to pharmacokinetics (PK) and pharmacodynamics (PD). To this end, ADMET profiling serves as a critical step in reducing attrition rates during preclinical and clinical stages.⁸³ ADMET property profiling also provides critical insights into the PK and safety profiles of compounds identified as potentially active against the selected respiratory viral targets. ADMET profiling provides early indications of potential safety issues, including hepatotoxicity, cardiotoxicity, and drug–drug interactions. These factors are particularly relevant for antiviral therapies, which are often administered in combination with other treatments. Maintaining sufficient plasma concentrations within the therapeutic window is critical for inhibiting viral

replication effectively while minimizing toxicity and preventing resistance. Key PK parameters, such as the volume of distribution (VD) and clearance (Cl) significantly influence a compound's antiviral effectiveness.⁸⁴

For all 339 040 compounds in the VS data set (see Table 2) forty-one ADMET properties were calculated using ADMET-AI (see Methods Section 2.9 for further details). This detailed profiling is included in the structure file of the VS data set to facilitate a comprehensive evaluation of candidate molecules. The user of the newly assembled and designed libraries is free to use other tools to estimate the ADMET profile of the newly assembled and designed libraries (see Section 3.9).

3.8 Machine learning-driven antiviral libraries targeting respiratory viruses

The classification step enabled the identification of 398 promising compounds with a high likelihood of antiviral activity, which were subsequently organized into seven focused libraries for each target. These libraries aim to streamline the



Table 6 Distance to model performance of the retraining data set, the best classification model, and consensus model for each selected target, attired by physicochemical properties

Range	IAV_polymerase (PA)			SARS-CoV-2_Mpro		
	Total	Best model (actives)	Consensus (actives)	Total	Best model (actives)	Consensus (actives)
Out	1360	95	34	85	56	44
Q1	78 691	5356	2298	102 608	74 364	51 313
Q2	83 268	5609	2276	54 992	39 935	27 668
Q3	97 040	6262	2614	85 659	62 136	42 693
Q4	78 681	4973	2012	95 696	69 459	47 716
Range	HRV_rotease			IAV_neuraminidase		
	Total	Best model (actives)	Consensus (actives)	Total	Best model (actives)	Consensus (actives)
Out	909	817	628	846	332	17
Q1	74 326	66 105	49 283	58 267	22 808	1386
Q2	87 034	77 425	57 813	86 483	33 667	2054
Q3	90 649	80 835	60 465	101 979	40 126	2428
Q4	86 122	76 967	57 562	91 465	36 167	2216
Range	IAV_M2 proton channel			IBV_neuraminidase		
	Total	Best model (actives)	Consensus (actives)	Total	Best model (actives)	Consensus (actives)
Out	7	7	4	13 563	6500	37
Q1	46 163	44 539	30 710	84 952	40 397	262
Q2	56 607	54 556	37 522	55 476	26 488	176
Q3	74 969	72 264	49 778	87 531	42 181	257
Q4	161 294	155 443	107 737	97 518	46 519	322
Range	SARS-CoV_Mpro					
	Total	Best model (actives)	Consensus (actives)			
Out	1709	274	77			
Q1	66 411	9898	3346			
Q2	85 126	12 495	4255			
Q3	90 323	13 285	4407			
Q4	95 471	14 040	4575			

Table 7 Number of active compounds from the newly designed antiviral-focused libraries for each target across quartiles

Quartile	HRV_protease	IAV_M2 proton channel	IAV_neuraminidase	IAV_polymerase (PA)	IBV_neuraminidase	SARS-CoV_Mpro	SARS-CoV-2_Mpro
Q1	268	126	—	—	—	2	2
Q2	2469	4484	1	16	—	597	1
Q3	19 317	5948	611	410	—	9526	9622
Q4	201 730	2518	7454	8683	57	6480	159 213
Out	1934	220	35	125	997	55	592

prioritization of candidates for further experimental validation or biological testing and are publicly accessible at https://github.com/DIFACQUIM/antiviral_ML.

To provide a comprehensive overview of the compounds and take all analysis and predictions together, eight distinct libraries focused on respiratory viruses were designed: the VS data set in conjunction with its predictions and seven subsets for each target. Each library is annotated with: “Canonical SMILES, Murcko SMILES, identifier (ID), database (DB),

number of repetitions, prediction label (for each model), prediction score (for each model), Quartile Pairsim (structural), Quartile (structural), Quartile Distance (physicochemical properties), Quartile (physicochemical properties)” plus the ADMET profile in the VS data set library.

Fig. 7 shows the chemical structures of representative compounds included in the newly generated antiviral-focused libraries. Specifically, the figure highlights predicted active compounds for four selected antiviral targets, with high



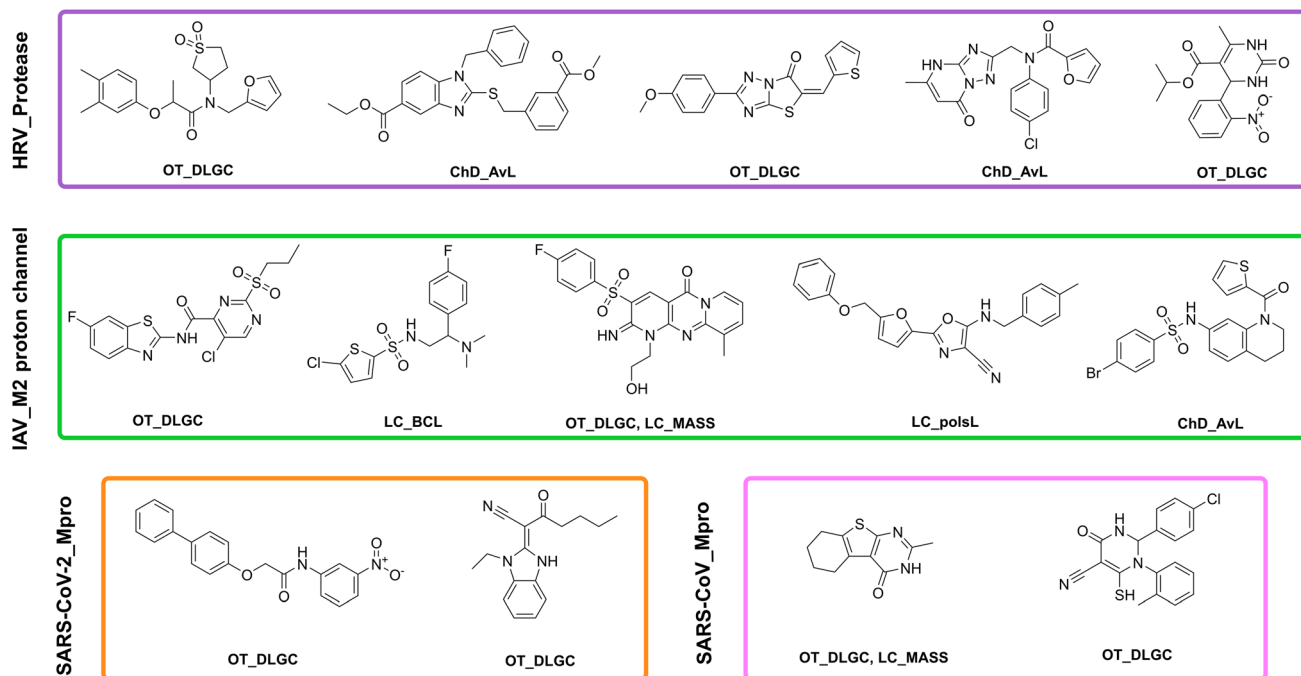


Fig. 7 Chemical structures of Q1 compounds (top five for targets HRV_protease and IAV_M2 proton channel) attired by Morgan Chiral of radius 2 (2048 bits) fingerprint. The label below each structure represents the acronym of each library as stated in Table 2.

predictive confidence (e.g., predictions within the first quartile (Q1) of the distance to model as described in Section 3.6). Notably, the presence of nitrogen atoms across all illustrated compounds aligns with the findings discussed in Section 3.3.2, emphasizing its relevance to antiviral activity.

Fig. S8 in the ESI† illustrates the chemical space distribution of top predicted active compounds, specifically those with the highest prediction confidence (Q1, as detailed in Table 7), across the newly designed target-focused libraries. These visualizations, generated using *t*-SNE based on the Morgan Chiral of radius 2 (2048 bits) fingerprint, highlight the structural diversity of Q1 compounds.

Notably, certain libraries lack Q1 compounds entirely, while libraries such as HRV protease and IAV M2 proton channel exhibit broader structural diversity, as reflected by the dispersed distribution of Q1 compounds, moreover, SARS-CoV-2 Mpro library, shows clustering, indicating structural similarity among predicted actives. This analysis underscores variability in structural diversity across libraries, suggesting that improvements in library design and model training could enhance the identification of high-confidence active compounds.

4 Conclusions

Herein we designed seven compound libraries with prospective antiviral activity, targeting respiratory viruses. The libraries were assembled and designed using available data in ChEMBL and predictive ML models. The designed libraries target specific antiviral targets: M2 proton channel of IAV, Mpro of SARS-CoV and SARS-CoV-2, neuraminidase of IAV and IBV, polymerase of IAV, and protease of HRV. Additionally, we report the results of

a cheminformatics analysis of the training compounds to assess their drug-like properties and scaffold diversity, comparing these features with those of approved antiviral drugs. The analysis revealed that training compounds exhibited favorable drug-like physicochemical properties. Scaffold analysis of the most frequent scaffolds from the construction of the ML models data set indicated that compounds targeting HRV protease and IAV M2 proton channel share at least one scaffold with the set of approved antivirals. Furthermore, compounds targeting neuraminidases of influenza A and B exhibited common scaffolds, predominantly single-ring structures. Analysis of the chemical space based on different fingerprint representations emphasized the large diversity of compounds with activity against SARS-CoV-2 Mpro and IAV neuraminidase.

For the seven antiviral target data sets with high model-ability, we developed ML predictive models, which showed improved MCC values after retraining. Among these, the AdaBoost model for IBV neuraminidase demonstrated the best performance. Overall, consensus ML models outperformed individual models, particularly for targets with larger and more balanced data sets. Compounds within the top confidence predictions from the seven newly designed antiviral-focused libraries represent strong candidates for further screening, including biological testing, which is the next step of this study from the wet lab experimental point of view. All seven antiviral-focused libraries developed in this study are freely available at https://github.com/DIFACQUIM/antiviral_ML for the scientific community to select, acquire, and biologically test the chemical libraries. To facilitate the use of these databases, each compound is annotated with confidence predictions and ADMET property profiles.



Abbreviations

ADASYN	Adaptive synthetic sampling
ADMET	Absorption, distribution, metabolism, excretion, and toxicity
AI	Artificial intelligence
API	Application programming interface
ARD	Acute respiratory disease
AUC	Area under the curve
BA	Balanced accuracy
CADD	Computer-aided drug design
Cl	Clearance
CSP3	Fraction of sp ³ carbon atoms
ECFP	Extended connectivity fingerprint
FCoV	Feline coronavirus
GTM	Generative topographic mapping
HBA	H-bond acceptors
HBD	H-bond donors
HEV-71	Enterovirus A71
HCoV-229E	Human coronavirus 229E
HCoV-NL63	Human coronavirus NL63
HIV	Human immunodeficiency virus
HPIV-1	Human parainfluenza virus 1
HRV	Human rhinovirus
HRSV	Human respiratory syncytial virus
IAV	<i>Influenza A virus</i>
IBV	<i>Influenza B virus</i>
JAK	Janus kinase
log <i>P</i>	Partition coefficient octanol/water
MACCS	Molecular ACCess system
MCC	Matthew's correlation coefficient
MERS	Middle East respiratory syndrome
MERS-CoV	Middle East respiratory syndrome coronavirus
ML	Machine learning
MODI	Modelability index
MOE	Molecular operating environment
Mpro	Main protease
MW	Molecular weight
NiV	<i>Henipavirus nipahense</i>
NPs	Natural products
PD	Pharmacodynamics
PK	Pharmacokinetics
PLP	Papain like-protease
PHEIC	Public health emergencies of international concern
R&D	Research and development
RdKit	Rational discovery kit
RdRp	RNA dependent RNA polymerase
RSV	Respiratory syncytial virus
RVs	Rhinoviruses
SARS	Severe acute respiratory syndrome
SARS-CoV	Severe acute respiratory syndrome coronavirus
SARS-CoV-2	Severe acute respiratory syndrome coronavirus 2
SMILES	Simplified molecular input line entry system
TPSA	Topological polar surface area

<i>t</i> -SNE	<i>t</i> -Distributed stochastic neighbor embedding
VD	Volume of distribution
VS	Virtual screening
WHO	World Health Organization

Data availability

The antiviral focused libraries generated in this study and the project code are available in ZENODO: <https://doi.org/10.5281/zenodo.15131233>. Supplementary figures and tables are included in a ESI file.†

Author contributions

Gabriela Valle-Núñez: methodology, software, validation, formal analysis, investigation, visualization, writing – original draft, writing – review & editing. Raziel Cedillo-González: conceptualization, data acquisition and curation, methodology, visualization, software, formal analysis, writing – original draft, writing – review & editing. Juan F. Avellaneda-Tamayo: conceptualization, methodology, software, supervision, formal analysis, writing – original draft, writing – review & editing. Fernanda I. Saldívar-González: conceptualization, methodology, software, formal analysis, writing – original draft, writing – review & editing. Diana L. Prado-Romero: conceptualization, methodology, software, formal analysis, writing – original draft, writing – review & editing. José L. Medina-Franco: conceptualization, formal analysis, investigation, resources, writing – review & editing, supervision, project administration, funding acquisition.

Conflicts of interest

The authors declare no competing financial interest.

Acknowledgements

We are grateful for the support of DGAPA, UNAM, Programa de Apoyo a Proyectos de Investigación e Innovación Tecnológica (PAPIIT), grant no. IV200121. R. C.-G., J. F. A.-T., F. I. S.-G. and D. L. P.-R. thank Consejo Nacional de Humanidades, Ciencias y Tecnologías (CONAHCyT), Mexico, for the postgraduate scholarships 1099206, 1270553, 848061, and 888207, respectively. Helpful discussions with Felipe Victoria-Muñoz are greatly acknowledged. We also thank Pedro A. Laurel-García for sharing the code to use ADMET-AI.

References

- 1 S. Kausar, F. S. Khan, M. I. M. Ur Rehman, M. Akram, M. Riaz, G. Rasool, A. H. Khan, I. Saleem, S. Shamim and A. Malik, *Int. J. Immunopathol. Pharmacol.*, 2021, **35**, 20587384211002621, DOI: [10.1177/20587384211002621](https://doi.org/10.1177/20587384211002621).
- 2 R. E. Baker, A. S. Mahmud, I. F. Miller, M. Rajeev, F. Rasambainarivo, B. L. Rice, S. Takahashi, A. J. Tatem, C. E. Wagner, L.-F. Wang, A. Wesolowski and



- C. J. E. Metcalf, *Nat. Rev. Microbiol.*, 2022, **20**, 193–205, DOI: [10.1038/s41579-021-00639-z](https://doi.org/10.1038/s41579-021-00639-z).
- 3 Prioritizing Diseases for Research and Development in Emergency Contexts, <https://www.who.int/activities/prioritizing-diseases-for-research-and-development-in-emergency-contexts>, accessed 15 May 2024.
- 4 Pathogens Prioritization. A Scientific Framework for Epidemic and Pandemic Research Preparedness, https://cdn.who.int/media/docs/default-source/consultation-rdb/prioritization-pathogens-v6final.pdf?sfvrsn=c98effa7_7&download=true, accessed 17 December 2024.
- 5 S. Katz, *Overview of Viral Respiratory Infections*, <https://www.msmanuals.com/professional/infectious-diseases/respiratory-viruses/overview-of-viral-respiratory-infections>, accessed 21 January 2025.
- 6 About Respiratory Illnesses, <https://www.cdc.gov/respiratory-viruses/about/index.html#:~:text=Everyyearrespiratoryvirusesuch,fallandwintervirusseason>, accessed 21 January 2025.
- 7 G. Mathez and V. Cagno, *Int. J. Mol. Sci.*, 2023, **24**, 13500, DOI: [10.3390/ijms241713500](https://doi.org/10.3390/ijms241713500).
- 8 T. Majerová and J. Konvalinka, *Mol. Aspects Med.*, 2022, **88**, 101159, DOI: [10.1016/j.mam.2022.101159](https://doi.org/10.1016/j.mam.2022.101159).
- 9 J. B. Mahony, A. Petrich and M. Smieja, *Crit. Rev. Clin. Lab Sci.*, 2011, **48**, 217–249, DOI: [10.3109/10408363.2011.640976](https://doi.org/10.3109/10408363.2011.640976).
- 10 A. Fendrick, A. Monto, B. Nightengale and M. Sarnes, *Arch. Intern. Med.*, 2003, **163**, 487–494, DOI: [10.1001/archinte.163.4.487](https://doi.org/10.1001/archinte.163.4.487).
- 11 N. Zhang, L. Wang, X. Deng, R. Liang, M. Su, C. He, L. Hu, Y. Su, J. Ren, F. Yu, L. Du and S. Jiang, *J. Med. Virol.*, 2020, **92**, 408–417, DOI: [10.1002/jmv.25674](https://doi.org/10.1002/jmv.25674).
- 12 A. Fitero, S. G. Bungau, D. M. Tit, L. Endres, S. A. Khan, A. F. Bungau, I. Romanul, C. M. Vesa, A.-F. Radu, A. G. Tarce, M. A. Bogdan, A. C. Nechifor and N. Negrut, *Int. J. Clin. Pract.*, 2022, **2022**, 1571826, DOI: [10.1155/2022/1571826](https://doi.org/10.1155/2022/1571826).
- 13 L. A. De Jesús-González, M. León-Juárez, F. I. Lira-Hernández, B. Rivas-Santiago, M. A. Velázquez-Cervantes, I. M. Méndez-Delgado, D. I. Macías-Guerrero, J. Hernández-Castillo, X. Hernández-Rodríguez, D. N. Calderón-Sandate, W. S. Mata-Martínez, J. M. Reyes-Ruíz, J. F. Osuna-Ramos and A. C. García-Herrera, *Pathogens*, 2024, **14**, 20, DOI: [10.3390/pathogens14010020](https://doi.org/10.3390/pathogens14010020).
- 14 D. Chattopadhyay and T. N. Naik, *Mini Rev. Med. Chem.*, 2007, **7**, 275–301, DOI: [10.2174/138955707780059844](https://doi.org/10.2174/138955707780059844).
- 15 S. K. Kim, T. S. Vo and D. H. Ngo, in *Advances in Food and Nutrition Research*, ed. S.-K. Kim, Academic Press, 2011, vol. 64, pp. 245–254, DOI: [10.1016/B978-0-12-387669-0.00019-3](https://doi.org/10.1016/B978-0-12-387669-0.00019-3).
- 16 Y. Guo, A. Ma, X. Wang, C. Yang, X. Chen, G. Li and F. Qiu, *Front. Chem.*, 2022, **10**, 1005360, DOI: [10.3389/fchem.2022.1005360](https://doi.org/10.3389/fchem.2022.1005360).
- 17 K. A. El Sayed, in *Studies in Natural Products Chemistry*, ed. A. ur-Rahman, Elsevier, 2000, part E, vol. 24, pp. 473–572, DOI: [10.1016/S1572-5995\(00\)80051-4](https://doi.org/10.1016/S1572-5995(00)80051-4).
- 18 S. Peng, H. Wang, Z. Wang and Q. Wang, *Molecules*, 2022, **27**, 7370, DOI: [10.3390/molecules27217370](https://doi.org/10.3390/molecules27217370).
- 19 P. Mehrbod, D. Hudy, D. Shyntum, J. Markowski, M. J. Los and S. Ghavami, *Biomolecules*, 2021, **11**, 10, DOI: [10.3390/biom11010010](https://doi.org/10.3390/biom11010010).
- 20 K. Liu, Y. Zhu, X. Cao, Y. Liu, R. Ying, Q. Huang, P. Gao and C. Zhang, *Heliyon*, 2023, **9**, e21648.
- 21 H. Liu, F. Ye, Q. Sun, H. Liang, C. Li, S. Li, R. Lu, B. Huang, W. Tan and L. Lai, *J. Enzyme Inhib. Med. Chem.*, 2021, **36**, 497–503, DOI: [10.1080/14756366.2021.1873977](https://doi.org/10.1080/14756366.2021.1873977).
- 22 E. Gayozo and L. Rojas, *Rev. Soc. Cient. del Parag.*, 2022, **27**, 101–121, DOI: [10.32480/rscp.2022.27.2.101](https://doi.org/10.32480/rscp.2022.27.2.101).
- 23 N. A. Ashour, A. A. Elmaaty, A. A. Sarhan, E. B. Elkaeed, A. M. Moussa, I. A. Erfan and A. A. Al-Karmalawy, *Drug Des., Dev. Ther.*, 2022, **16**, 685–715, DOI: [10.2147/DDDT.S354841](https://doi.org/10.2147/DDDT.S354841).
- 24 D. A. Winkler, *J. Mater. Chem.*, 2024, **62**, 2844–2879, DOI: [10.1007/s10910-023-01568-3](https://doi.org/10.1007/s10910-023-01568-3).
- 25 Q. Liao, Z. Chen, Y. Tao, B. Zhang, X. Wu, L. Yang, Q. Wang and Z. Wang, *Sci. Rep.*, 2021, **11**, 22796, DOI: [10.1038/s41598-021-02266-3](https://doi.org/10.1038/s41598-021-02266-3).
- 26 K. Klimenko, G. Marcou, D. Horvath and A. Varnek, *J. Chem. Inf. Model.*, 2016, **56**, 1438–1454, DOI: [10.1021/acs.jcim.6b00192](https://doi.org/10.1021/acs.jcim.6b00192).
- 27 J. V. de Julián-Ortiz, J. Gálvez, C. Muñoz-Collado, R. García-Domenech and C. Gimeno-Cardona, *J. Med. Chem.*, 1999, **42**, 3308–3314, DOI: [10.1021/jm981132u](https://doi.org/10.1021/jm981132u).
- 28 P. Richardson, I. Griffin, C. Tucker, D. Smith, O. Oechsle, A. Phelan, M. Rawling, E. Savory and J. Stebbing, *Lancet*, 2020, **395**, e30–e31, DOI: [10.1016/S0140-6736\(20\)30304-4](https://doi.org/10.1016/S0140-6736(20)30304-4).
- 29 P. Ranjan, J. Rani, U. Sahoo, A. Nayak and P. Kumar, *Pharm. Innov.*, 2023, **12**, 1070–1073.
- 30 E. S. Istifli, N. Okumus, C. Sarikurku, E. R. Kuhn, P. A. Netz and A. S. Tepe, *J. Biomol. Struct. Dyn.*, 2023, **42**, 8202–8214, DOI: [10.1080/07391102.2023.2267696](https://doi.org/10.1080/07391102.2023.2267696).
- 31 K. Srivastava and M. K. Singh, *Metab. Open*, 2021, **12**, 100121, DOI: [10.1016/j.metop.2021.100121](https://doi.org/10.1016/j.metop.2021.100121).
- 32 C. Wilson, J. M. F. Gardner, D. W. Gray, B. Baragana, P. G. Wyatt, A. Cookson, S. Thompson, C. Mendoza-Martinez, M. J. Bodkin, I. H. Gilbert and G. J. Tarver, *PLoS Neglected Trop. Dis.*, 2023, **17**, e0011799, DOI: [10.1371/journal.pntd.0011799](https://doi.org/10.1371/journal.pntd.0011799).
- 33 F. Potlitz, A. Link and L. Schulig, *Expert Opin. Drug Discovery*, 2023, **18**, 303–313, DOI: [10.1080/17460441.2023.2171984](https://doi.org/10.1080/17460441.2023.2171984).
- 34 J. Kuan, M. Radaeva, A. Avenido, A. Cherkasov and F. Gentile, *Wiley Interdiscip. Rev.: Comput. Mol. Sci.*, 2023, **13**, e1678, DOI: [10.1002/wcms.1678](https://doi.org/10.1002/wcms.1678).
- 35 A. Gryniukova, F. Kaiser, I. Myziuk, D. Aliksieieva, C. Leberecht, P. P. Heym, O. O. Tarkhanova, Y. S. Moroz, P. Borysko and V. J. Haupt, *J. Med. Chem.*, 2023, **66**, 10241–10251, DOI: [10.1021/acs.jmedchem.3c00128](https://doi.org/10.1021/acs.jmedchem.3c00128).
- 36 F. I. Saldívar-González, G. Navarrete-Vázquez and J. L. Medina-Franco, *Front. Pharmacol.*, 2023, **14**, 1276444, DOI: [10.3389/fphar.2023.1276444](https://doi.org/10.3389/fphar.2023.1276444).
- 37 B. Zdrzil, E. Felix, F. Hunter, E. J. Manners, J. Blackshaw, S. Corbett, M. de Veij, H. Ioannidis, D. M. Lopez, J. F. Mosquera, M. P. Magarinos, N. Bosc, R. Arcila, T. Kizilören, A. Gaulton, A. P. Bento, M. F. Adasme,



- P. Monecke, G. A. Landrum and A. R. Leach, *Nucleic Acids Res.*, 2024, **52**, D1180–D1192, DOI: [10.1093/nar/gkad1004](https://doi.org/10.1093/nar/gkad1004).
- 38 M. Davies, M. Nowotka, G. Papadatos, N. Dedman, A. Gaulton, F. Atkinson, L. Bellis and J. P. Overington, *Nucleic Acids Res.*, 2015, **43**, W612–W620, DOI: [10.1093/nar/gkv352](https://doi.org/10.1093/nar/gkv352).
- 39 D. Weininger, *J. Chem. Inf. Comput. Sci.*, 1988, **28**, 31–36, DOI: [10.1021/ci00057a005](https://doi.org/10.1021/ci00057a005).
- 40 D. S. Wishart, Y. D. Feunang, A. C. Guo, E. J. Lo, A. Marcu, J. R. Grant, T. Sajed, D. Johnson, C. Li, Z. Sayeeda, N. Assempour, I. Iynkkaran, Y. Liu, A. Maciejewski, N. Gale, A. Wilson, L. Chin, R. Cummings, D. Le, A. Pon, C. Knox and M. Wilson, *Nucleic Acids Res.*, 2018, **46**, D1074–D1082, DOI: [10.1093/nar/gkx1037](https://doi.org/10.1093/nar/gkx1037).
- 41 G. Landrum, *RDKit*, <https://www.rdkit.org/>, accessed 7 November 2024.
- 42 *MolVS: Molecule Validation and Standardization — MolVS 0.1.1 documentation*, <https://molvs.readthedocs.io/en/latest/>, accessed 7 November 2024.
- 43 N. Sánchez-Cruz, B. A. Pilón-Jiménez and J. L. Medina-Franco, *F1000Research*, 2020, **8**, 2071, DOI: [10.12688/f1000research.21540.2](https://doi.org/10.12688/f1000research.21540.2).
- 44 A. Golbraikh, E. Muratov, D. Fourches and A. Tropsha, *J. Chem. Inf. Model.*, 2014, **54**, 1–4, DOI: [10.1021/ci400572x](https://doi.org/10.1021/ci400572x).
- 45 J. L. Durant, B. A. Leland, D. R. Henry and J. G. Nourse, *J. Chem. Inf. Comput. Sci.*, 2002, **42**, 1273–1280, DOI: [10.1021/ci010132r](https://doi.org/10.1021/ci010132r).
- 46 D. Rogers and M. Hahn, *J. Chem. Inf. Model.*, 2010, **50**, 742–754, DOI: [10.1021/ci100050t](https://doi.org/10.1021/ci100050t).
- 47 N. Sánchez-Cruz and J. L. Medina-Franco, *J. Med. Chem.*, 2021, **64**, 8208–8220.
- 48 *Molecular Operating Environment (MOE)*, 2024.0601, Chemical Computing Group ULC, Sherbrooke St. W., Montreal, QC H3A 2R7, 2025, pp. 910–1010, <https://www.chemcomp.com/en/Research-Citing-MOE.htm>.
- 49 G. W. Bemis and M. A. Murcko, *J. Med. Chem.*, 1996, **39**, 2887–2893, DOI: [10.1021/jm9602928](https://doi.org/10.1021/jm9602928).
- 50 F. Pedregosa, G. Varoquaux, A. Gramfort, V. Michel, B. Thirion, O. Grisel, M. Blondel, A. Müller, J. Nothman, G. Louppe, P. Prettenhofer, R. Weiss, V. Dubourg, J. Vanderplas, A. Passos, D. Cournapeau, M. Brucher, M. Perrot and É. Duchesnay, arXiv [cs.LG], 2012, preprint, 1201.0490, DOI: [10.48550/arXiv.1201.0490](https://doi.org/10.48550/arXiv.1201.0490).
- 51 H. Mary, E. Noutahi, DomInvivo, L. Zhu, M. Moreau, S. Pak, D. Gilmour, S. Whitfield, t., Valence-JonnyHsu, H. Hounwanou, I. Kumar, S. Maheshkar, S. Nakata, K. M. Kovary, C. Wognum, M. Craig and D. Bot, *datamol-io/datamol: 0.12.3*, Zenodo, 2024, DOI: [10.5281/zenodo.10535844](https://doi.org/10.5281/zenodo.10535844).
- 52 C. A. Lipinski, F. Lombardo, B. W. Dominy and P. J. Feeney, *Adv. Drug Delivery Rev.*, 1997, **23**, 3–25, DOI: [10.1016/S0169-409X\(96\)00423-1](https://doi.org/10.1016/S0169-409X(96)00423-1).
- 53 M. Ali, *PyCaret: an open source, low-code machine learning library in Python*, <https://pycaret.org/>, accessed 7 November 2024.
- 54 H. He, Y. Bai, E. A. Garcia and S. Li, in *2008 IEEE International Joint Conference on Neural Networks (IEEE World Congress on Computational Intelligence)*, IEEE, 2008, pp. 1322–1328, DOI: [10.1109/IJCNN.2008.4633969](https://doi.org/10.1109/IJCNN.2008.4633969).
- 55 B. Ramsundar, P. E. P. Walters, and V. Pande, *Deep Learning for the Life Sciences*, O'Reilly Media, Sebastopol, CA, 2019.
- 56 *Splitters — Deepchem 2.8.1.dev Documentation*, https://deepchem.readthedocs.io/en/latest/api_reference/splitters.html#fingerprintsplitter, accessed 14 November 2024.
- 57 C. Miller, T. Portlock, D. M. Nyaga and J. M. O'Sullivan, *Front. Bioinform.*, 2024, **4**, 1457619, DOI: [10.3389/fbinf.2024.1457619](https://doi.org/10.3389/fbinf.2024.1457619).
- 58 *CORONAVIRUS Library*, <https://www.chemdiv.com/catalog/focused-and-targeted-libraries/coronavirus-library/>, accessed 30 August 2024.
- 59 *Antiviral Library*, <https://www.chemdiv.com/catalog/focused-and-targeted-libraries/antiviral-library/>, accessed 30 August 2024.
- 60 *Drug-Like Green Collection*, <https://www.otavachemicals.com/products/compound-libraries-for-hts/drug-like-green-collection>, accessed 28 November 2024.
- 61 *Antiviral Library*, <https://enamine.net/compound-libraries/targeted-libraries/antiviral-library?highlight=WyJhbnRpdmlmYWwvXQ==>, accessed 28 November 2024.
- 62 *Discovery Diversity Set*, https://chem-space.com/compounds/discovery_diversity_set, accessed 31 August 2024.
- 63 *Helicase Screening Libraries*, <https://lifechemicals.com/screening-libraries/targeted-and-focused-screening-libraries/helicase-focused-library>, accessed 28 November 2024.
- 64 *Antiviral Screening Compound Libraries*, <https://lifechemicals.com/screening-libraries/targeted-and-focused-screening-libraries/antiviral-libraries>, accessed 28 November 2024.
- 65 *DNA and RNA Polymerase Screening Libraries*, <https://lifechemicals.com/screening-libraries/targeted-and-focused-screening-libraries/polymerase-focused-libraries>, accessed 28 November 2024.
- 66 *Coronavirus Inhibitor Screening Libraries*, <https://lifechemicals.com/screening-libraries/targeted-and-focused-screening-libraries/coronavirus-screening-libraries>, accessed 28 November 2024.
- 67 *Coronavirus Inhibitor Screening Libraries*, <https://lifechemicals.com/screening-libraries/targeted-and-focused-screening-libraries/coronavirus-screening-libraries>, accessed 28 November 2024.
- 68 *Antiviral Screening Compound Libraries*, <https://lifechemicals.com/screening-libraries/targeted-and-focused-screening-libraries/antiviral-libraries>, accessed 28 November 2024.
- 69 *Antiviral Screening Compound Libraries*, <https://lifechemicals.com/screening-libraries/targeted-and-focused-screening-libraries/antiviral-libraries>, accessed 28 November 2024.
- 70 *Antiviral Screening Compound Libraries*, <https://lifechemicals.com/screening-libraries/targeted-and-focused-screening-libraries/antiviral-libraries>, accessed 28 November 2024.



- [screening-libraries/antiviral-libraries](#), accessed 28 November 2024.
- 71 *Pre-plated Focused Libraries*, <https://lifechemicals.com/screening-libraries/pre-plated-focused-libraries>, accessed 28 November 2024.
- 72 *Coronavirus Inhibitor Screening Libraries*, <https://lifechemicals.com/screening-libraries/targeted-and-focused-screening-libraries/coronavirus-screening-libraries>, accessed 28 November 2024.
- 73 *Coronavirus Inhibitor Screening Libraries*, <https://lifechemicals.com/screening-libraries/targeted-and-focused-screening-libraries/coronavirus-screening-libraries>, accessed 28 November 2024.
- 74 I. Sushko, S. Novotarskyi, R. Körner, A. K. Pandey, A. Cherkasov, J. Li, P. Gramatica, K. Hansen, T. Schroeter, K.-R. Müller, L. Xi, H. Liu, X. Yao, T. Öberg, F. Hormozdiari, P. Dao, C. Sahinalp, R. Todeschini, P. Polishchuk, A. Artemenko, V. Kuz'min, T. M. Martin, D. M. Young, D. Fourches, E. Muratov, A. Tropsha, I. Baskin, D. Horvath, G. Marcou, C. Muller, A. Varnek, V. V. Prokopenko and I. V. Tetko, *J. Chem. Inf. Model.*, 2010, **50**, 2094–2111, DOI: [10.1021/ci100253r](#).
- 75 K. Swanson, P. Walther, J. Leitz, S. Mukherjee, J. C. Wu, R. V. Shivnaraine and J. Zou, *Bioinformatics*, 2024, **40**, btac416, DOI: [10.1093/bioinformatics/btac416](#).
- 76 *admet_ai: Training and Prediction Scripts for Chemprop Models Trained on ADMET Datasets*, Github, https://github.com/swansonk14/admet_ai, accessed 28 November 2024.
- 77 Y. A. Shtyrya, L. V. Mochalova and N. V. Bovin, *Acta Naturae*, 2009, **1**, 26–32, DOI: [10.32607/20758251-2009-1-2-26-32](#).
- 78 C. Wang, Z. Song, H. Yu, K. Liu and X. Ma, *Acta Pharm. Sin. B*, 2015, **5**, 431–441, DOI: [10.1016/j.apsb.2015.07.002](#).
- 79 G. Ahmad, M. Sohail, M. Bilal, N. Rasool, M. U. Qamar, C. Ciurea, L. G. Marceanu and C. Misarca, *Molecules*, 2024, **29**, 2232, DOI: [10.3390/molecules29102232](#).
- 80 A. Mermer, T. Keles and Y. Sirin, *Bioorg. Chem.*, 2021, **114**, 105076, DOI: [10.1016/j.bioorg.2021.105076](#).
- 81 J. J. Naveja and J. L. Medina-Franco, *Front. Chem.*, 2019, **7**, 510, DOI: [10.3389/fchem.2019.00510](#).
- 82 J. L. Medina-Franco, J. R. Rodríguez-Pérez, H. F. Cortés-Hernández and E. López-López, *Artif. Intell. Life Sci.*, 2024, **6**, 100117, DOI: [10.1016/j.aills.2024.100117](#).
- 83 L. Strasfeld and S. Chou, *Infect. Dis. Clin. North Am.*, 2010, **24**, 413–437, DOI: [10.1016/j.idc.2010.01.001](#).
- 84 T. Chaira, C. Subramani and T. K. Barman, *Pharmaceutics*, 2023, **15**, 1212, DOI: [10.3390/pharmaceutics15041212](#).

